2D Materials

RECEIVED
4 August 2016

REVISED
3 October 2016

ACCEPTED FOR PUBLICATION
10 October 2016

PUBLISHED
20 October 2016

LETTER

Unsupported single-atom-thick copper oxide monolayers

Kuibo Yin[1,2,5], Yu-Yang Zhang[3,2,5], Yilong Zhou[1,5], Litao Sun[1,4], Matthew F Chisholm[2], Sokrates T Pantelides[3,2] and Wu Zhou[2,6]

[1] SEU-FEI Nano-Pico Center, Collaborative Innovation Center for Micro/Nano Fabrication, Device and System, Key Lab of MEMS of Ministry of Education, Southeast University, Nanjing 210096, People's Republic of China
[2] Materials Science & Technology Division, Oak Ridge National Laboratory, Oak Ridge, TN 37831, USA
[3] Department of Physics and Astronomy and Department of Electrical Engineering and Computer Science, Vanderbilt University, Nashville, TN 37235, USA
[4] Center for Advanced Materials and Manufacture, Joint Research Institute of Southeast University and Monash University, Suzhou 215123, People's Republic of China
[5] These authors contributed equally.
[6] Present Address: School of Physical Sciences, CAS Key Laboratory of Vacuum Physics, University of Chinese Academy of Sciences, Beijing 100049, People's Republic of China

E-mail: zhangyuyang.cn@gmail.com, slt@seu.edu.cn and wu.zhou.stem@gmail.com

Keywords: copper oxide, 2D materials, first-principles calculations, *in situ* STEM

Supplementary material for this article is available online

Abstract

Oxide monolayers may present unique opportunities because of the great diversity of properties of these materials in bulk form. However, reports on oxide monolayers are still limited. Here we report the formation of single-atom-thick copper oxide layers with a square lattice both in graphene pores and on graphene substrates using aberration-corrected scanning transmission electron microscopy. First-principles calculations find that CuO is energetically stable and its calculated lattice spacing matches well with the measured value. Furthermore, free-standing copper oxide monolayers are predicted to be semiconductors with band gaps ~3 eV. The new wide-bandgap single-atom-thick copper oxide monolayers usher a new frontier to study the highly diverse family of two-dimensional oxides and explore their properties and their potential for new applications.

Introduction

Among all two-dimensional (2D) crystals, monolayer (ML) oxides are an especially interesting class because of the many coupled degrees of freedom that are present in bulk oxides (charge, spin, lattice), to which quantum confinement is now added. We can, therefore, expect a wide spectrum of electronic and magnetic properties with potential for applications. Many efforts have been made to fabricate 2D oxides. Few-layer films have been successfully cleaved from bulk layered-oxides [1–4]. Mono- or few-layer oxides bonded to substrates have also been grown [5–8]. A recent report on ZnO monolayers suspended in a graphene pore presages a potentially exciting area of oxide monolayers [9].

Copper oxides are unique among metal oxides because they are the only ones in which the metal atom has a full d-shell. They have received a great deal of attention due to their versatile applications in high-temperature superconductivities [10–13], supported catalysts [14], solar cells [15], thin-film transistors [16], and so on. The oxidation of the top layer of a copper substrate, i.e. a supported copper-oxide thin film, has also been extensively studied [17–20]. Recently, a superior visible-light-conversion efficiency was reported for a four-atom-thick Cu_2O film photoelectrode [21]. Although a monolayer structure is particularly useful in elucidating the nature of active catalytic sites [14, 21], the synthesis of an unsupported single-atom-thick copper-oxide monolayer has remained a challenge [22, 23].

In this paper, we report the formation of single-atom-thick copper oxide monolayers under electron beam irradiation. Small clusters of copper oxide were driven by a 60 keV electron beam to form monolayer nanosheets with a square Cu sub-lattice, either spanning graphene pores to form unsupported monolayer

oxide membranes or being supported on the graphene surface. The exclusive presence of Cu and O was confirmed by local chemical analysis via electron-energy-loss spectroscopy (EELS). Quantum mechanical calculations find that both CuO and Cu_2O square monolayer are possible while CuO is more stable than Cu_2O in energy. Moreover, comparing the Cu–Cu distance in the fabricated sample with a statistical analysis to the calculated Cu–Cu distance using a state-of-the-art exchange-correlation functional, we conclude that the as-fabricated sample is CuO monolayer. Theoretical calculations also indicate that free-standing CuO and Cu_2O monolayers are stable. They are wide-bandgap semiconductors with band gaps ~3 eV. The stoichiometry variation changes the bandgap from indirect for CuO monolayer to direct for Cu_2O monolayer, suggesting that the electronic and optical properties of monolayer oxidized copper can be tuned by the oxygen content.

Results and discussion

Formation of CuO monolayer on graphene substrate

A schematic diagram of the *in situ* formation process for the supported monolayer CuO membrane is shown in figure 1(a). Initially, the sample preparation and process method that we used generates numerous small copper oxide clusters (smaller than 2 nm in diameter) and isolated Cu atoms on the graphene layer, mostly attached to the step edges of multilayer graphene patches (see methods and supplementary figure S1). A typical scanning transmission electron microscopy (STEM) annular dark field (ADF) image of small copper oxide clusters on a graphene surface is shown in figure 1(b). Chemical analysis via EELS showed the presence of oxygen and copper, as illustrated in supplementary figure S2. These small copper oxide clusters are mobile around the graphene edges and their morphology changes constantly under electron irradiation. Under prolonged low-dose-rate irradiation by a scanning focused 60 keV electron beam, these small copper-oxide clusters can transform into a crystalline monolayer structure, with the Cu atoms forming a square sub-lattice (figures 1(c), (d) and supplementary figure S3).

Measurements of the Cu sub-lattice show a lattice constant of 2.69 ± 0.05 Å for the monolayer structure (see supplementary figure S4). For simplicity, we define a square unit cell with $\langle 100 \rangle^s$ along the square edge. Quantitative STEM-ADF image analysis suggests that the monolayer nanosheets are single-atom-thick, as the image intensity from the Cu sub-lattice is equivalent to a single Cu atom on graphene. In order to analyze the composition of the observed monolayer crystals, we acquired local EELS by scanning the electron beam over 2 nm × 1 nm regions inside the nanosheets. As shown in figure 1(e) and supplementary figure S5, both copper and oxygen signals were detected, as evidenced by the Cu M-edge at ~78 eV and O K-edge at 532 eV. Other light elements, such as B, N, and F, were not detected. Considering the large energy transfer to H by the electron beam 'collision' effect [24], a hydroxide cannot survive and can, therefore, be excluded. In addition density functional theory (DFT) calculations of a hydrogenated square CuO found that the structure has negative-frequency phonon modes and is, therefore, unstable. Elemental mapping further confirms that an oxygen signal is associated with the nanocrystal (supplementary figure S5), indicating that the observed monolayer crystal is copper oxide, but the precise stoichiometry cannot be determined from these measurements.

We carried out DFT calculations to further examine the copper oxide structure and stoichiometry. We find that 3D Cu clusters are energetically favored over a monolayer structure (see supplementary figure S6). This result and the experimental detection of O signals exclude the possibility that the observed 2D patch is a pure Cu sheet, although a membrane with similar square structure made of Fe atoms has been reported by Zhao *et al* [25]. In view of the presence of an O K-edge in the EELS data, two types of copper-oxide patches, supported on a graphene substrate, with different stoichiometry corresponding to the two common copper oxides were considered: cupric oxide (CuO) and cuprous oxide (Cu_2O). We used a $Cu_{36}O_{49}$ cluster for a 1:1 Cu–O ratio, with additional oxygen and hydrogen passivation on the edges, and similarly a $Cu_{36}O_{24}$ cluster for a 2:1 Cu–O ratio. Optimized structures are shown in figures 1(f) and (g). The projected Cu–Cu distance, d_{Cu-Cu}, in the center of the $Cu_{36}O_{49}$ and the $Cu_{36}O_{24}$ clusters are 2.67 Å and 2.47 Å, respectively. A comparison of these theoretical values with the experimental measurement of 2.69 ± 0.05 Å corroborates the fabricated monolayer is CuO. The accuracy of the calculated Cu–Cu distances in the two structures is attested by the corresponding calculated values for the 3D bulk materials (see methods and supplementary figure S8). The binding energy difference between a CuO patch and a Cu_2O patch on a graphene substrate is negligible (3 meV per Cu atom). Thus, we can determine which structure is energetically preferred by simply comparing their cohesive energies in free-standing form. Our calculations show that CuO is energetically preferred by 0.26 eV per Cu atom (μ_{Cu} is chosen from bulk Cu). As a result, the net conclusion is that the copper oxide patches on graphene are CuO.

The identification of the observed copper-oxide monolayer as CuO is further supported by the magnified view of the STEM-ADF image in figure S7, where light atoms are observed at the centers of most Cu square units, i.e., the observed structure resembles the schematic model of figure 3(a) (CuO) as opposed to that of figure 3(g) (Cu_2O). The few missing O atoms are probably knocked out by the electron beam.

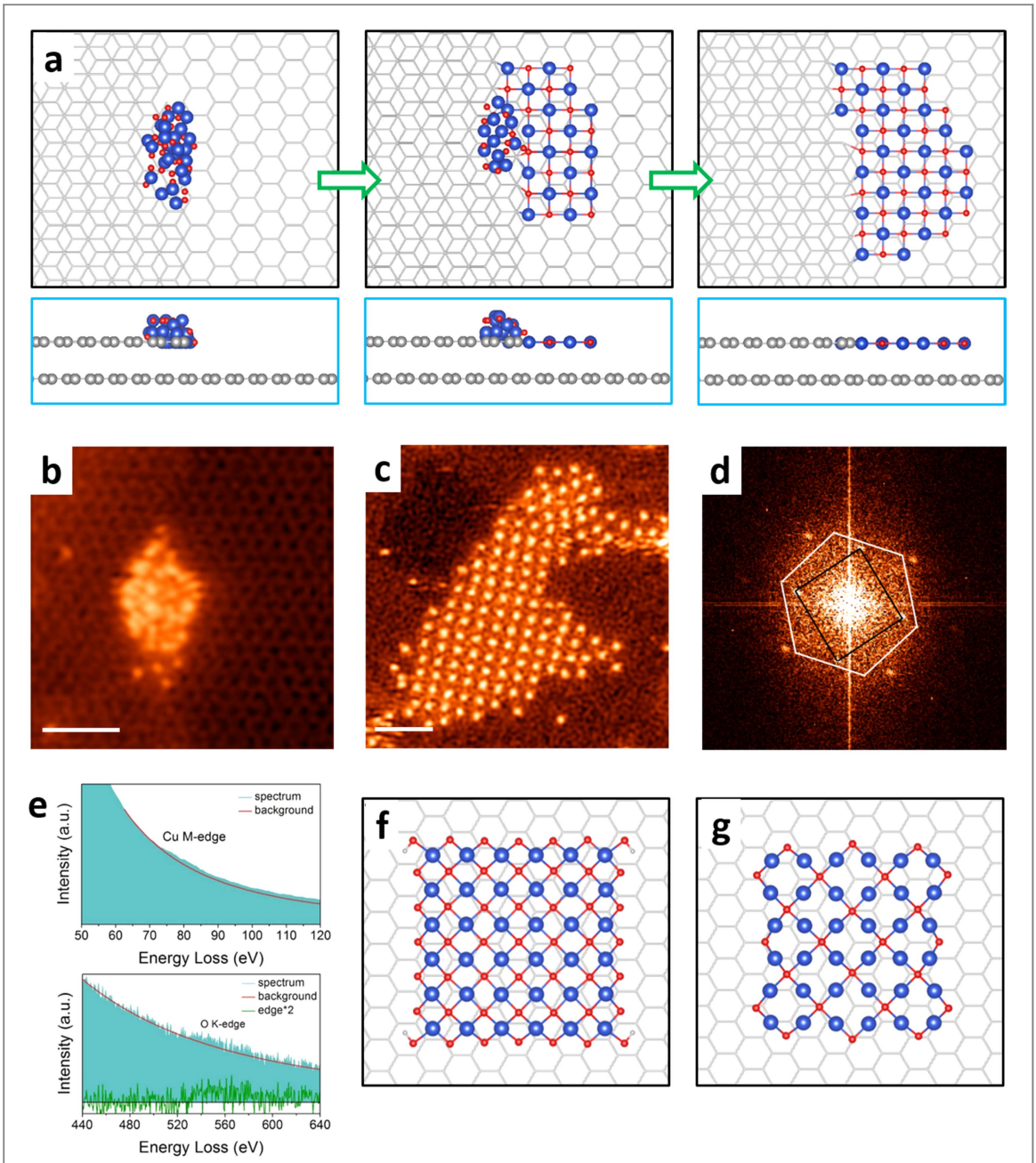

Figure 1. Monolayer CuO nanosheets on a graphene substrate. (a) Schematic of the formation process. The top panels are in top views and the bottom panels are in side views. (b) STEM-ADF image of a copper oxide cluster at the step edge of a graphene substrate. (c) STEM-ADF image of an ordered CuO monolayer nanosheet on a graphene substrate. (d) Fast Fourier Transformat (FFT) pattern of (c). (e) EELS taken from a 2 nm × 1 nm area in the CuO monolayer. The spectra were extracted from the spectrum image presented in supplementary figure S5. (f) Theoretical model of a $Cu_{36}O_{49}$ cluster on a graphene substrate. (g) Theoretical model of a $Cu_{36}O_{24}$ cluster on a graphene substrate. Blue balls are copper, red balls are oxygen and gray balls are carbon. Scale bars: 1 nm.

Formation of unsupported CuO monolayer in graphene pores

In addition to the formation of monolayer CuO nanosheets on a graphene substrate, unsupported CuO monolayers can form in graphene pores. Indeed, small copper oxide clusters near graphene pores (figure 2(a)) can form suspended membranes (figure 2(b)) under gentle electron irradiation. The STEM-ADF image in figure 2(b) and its corresponding FFT (figure 2(c)) show that the suspended monolayer crystal has a square Cu sub-lattice similar to those observed for supported CuO nanosheets, with a nearest Cu–Cu distance of ~2.65 Å. Both Cu and O EELS signals were detected from such suspended monolayers. We calculated the stability of a $Cu_{21}O_{12}$ nanosheet (representing CuO with Cu terminated edges) in a graphene nanopore. The optimized structure (as shown in figure 2(d)) shows a projected Cu–Cu distance of 2.70 Å, which is slightly larger than the calculated Cu–Cu distance of a CuO patch on graphene (2.67 Å), but is still close to the experimental value of ~2.65 Å. The $\langle 100 \rangle^s$ direction of the CuO monolayer aligns with the $\langle 11\bar{2} \rangle$ of the graphene lattice, which is also in agreement with the

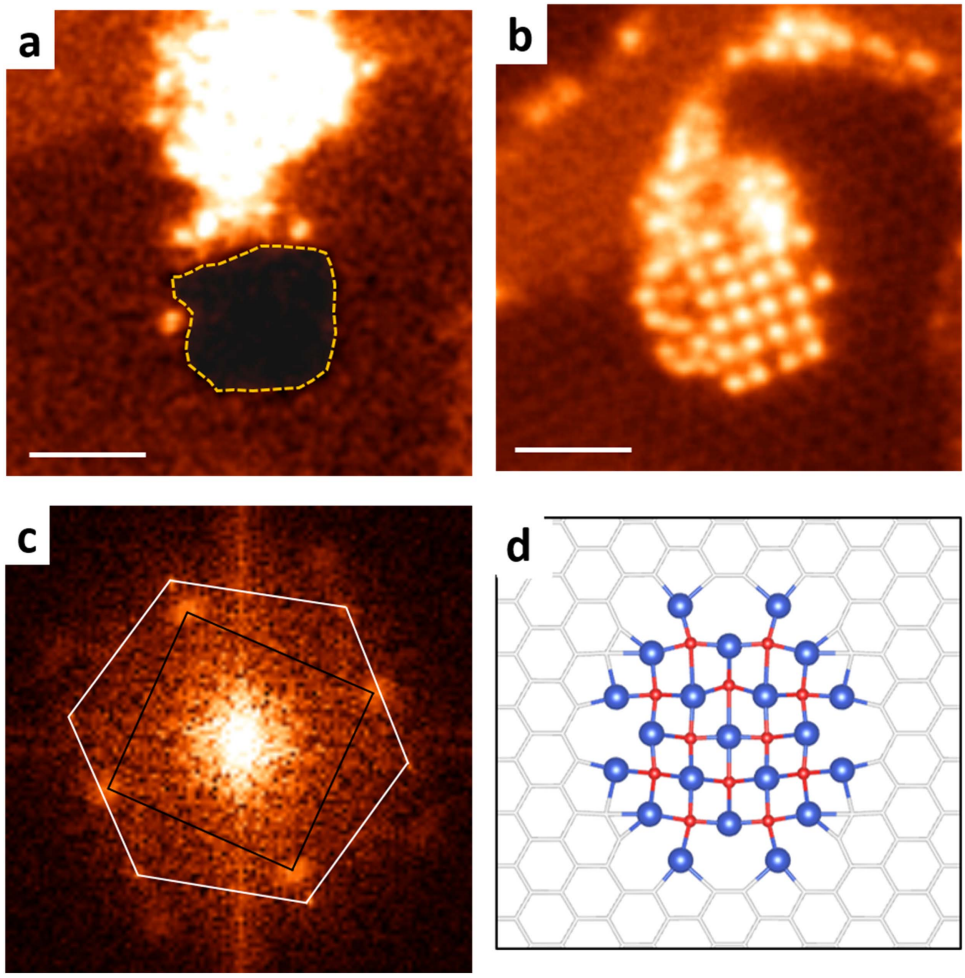

Figure 2. An unsupported monolayer CuO in a graphene pore. (a) A Cu oxide cluster at the edge of a graphene pore (highlighted). (b) A CuO monolayer suspended in a graphene pore. (c) FFT of (b), which shows the lattice relationship between graphene and copper oxide monolayer. (d) A theoretical model of a CuO membrane suspended in a graphene pore. Scale bars: 1 nm.

experimental observations. Furthermore, DFT calculations find that there are no negative-frequency phonon modes in this configuration, even though some geometric distortion at the CuO–graphene interface can be seen (the absence of negative-frequency phonon modes means that the structure is stable [26]). We, therefore, conclude that a suspended monolayer CuO patch can exist as a stable structure in a graphene pore.

Investigation of free-standing copper oxide monolayer

In order to further explore the formation of a stable free-standing copper-oxide monolayer, we examined the interaction between the observed CuO patch with the graphene substrate. DFT calculations find that the binding energy is 47 meV/Cu for the $Cu_{36}O_{49}$ cluster and 50 meV/Cu for the $Cu_{36}O_{24}$ cluster, respectively, indicating the presence of a van der Waals (vdW) interaction between the Cu_xO sheet and the graphene substrate. This weak vdW interaction as well as the formation of the unsupported monolayer CuO membrane suggest that a large-scale free-standing CuO monolayer could exist, and could potentially be grown at large scale using chemical methods and then be removed from the graphene substrate as a free-standing monolayer in a way similar to the transfer of graphene and transition-metal dichalcogenides. This hypothesis was further tested by DFT calculations using a state-of-the-art functional for the exchange-correlation potential. A stable planar CuO monolayer is found (figure 3(a)). This configuration maintains the same square lattice as the CuO membrane described above, with a projected Cu–Cu distance of 2.72 Å, which is also close to the experimental value (2.69 Å).

Similar to the low-temperature (<213 K) magnetic ordering in bulk CuO, monolayer CuO shows a D-type antiferromagnetic (AFM) ordering, in which magnetic stripes lie along the $[100]^s$ direction. However, monolayer CuO has a 3.37 eV indirect bandgap (figure 3(c)), which is significantly larger than the ~1.5 eV indirect bandgap in bulk CuO.

As also shown in bulk CuO, a CuO monolayer with similar structure but different magnetic ordering exists. Figure 3(d) shows the top view and side view of

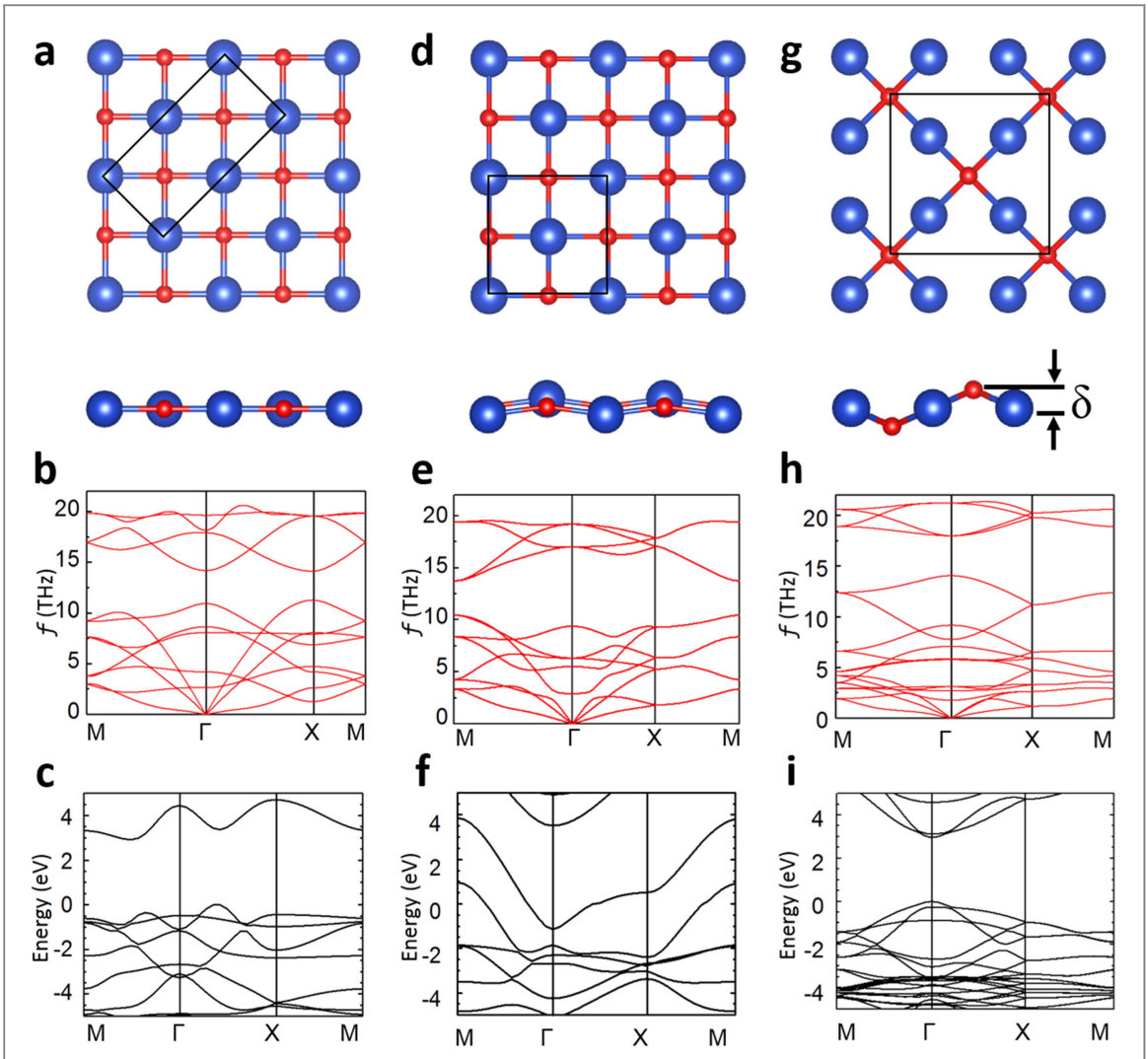

Figure 3. Theoretical calculations of freestanding copper oxide monolayer. (a)–(c) are for D-type CuO. (d)–(f) are for G-type CuO. (g)–(i) are for Cu_2O. (a), (d), and (g) are top views and side views of the atomic structures. (b), (e), and (h) are phonon dispersions. (c), (f), and (i) are energy band structures.

a configuration with G-type AFM order (magnetic strips are along the [110]^s direction). Compared with the planar D-type AFM CuO monolayer, a G-type AFM CuO monolayer is buckled with half of the Cu atoms residing above and the other half of the Cu atoms residing below the oxygen plane. Energetically, a CuO monolayer with G-type AFM order has higher energy than a CuO monolayer with D-type AFM by 0.20 eV per formula unit (f.u.), suggesting that a free-standing CuO monolayer grown under thermodynamically equilibrium conditions would adopt a D-type AFM ordering. But as there are no negative frequencies in its phonon modes (figure 3(e)), a CuO monolayer with G-type AFM order can also exist. The band structure calculations of CuO monolayer with G-type AFM order (figure 3(f)) indicate that the material is metallic. The semiconductor-to-metal transition from D-type AFM CuO monolayer to G-type AFM CuO monolayer caused by a slight structural change may be useful for future applications, such as force detectors.

DFT calculations also find a stable free-standing Cu_2O monolayer (figures 3(g) and (h)). In this configuration, O atoms sit above the Cu plane with a buckling distance of 0.49 Å. Comparing with a CuO monolayer, the oxygen atoms maintain fourfold coordination, but the copper atoms change to twofold coordination. $d_{Cu–Cu}$ shrinks from 2.72 Å in CuO monolayer to 2.54 Å (~7%). Different from the multiple AFM orderings in the CuO monolayer, a Cu_2O monolayer is not spin polarized (paramagnetic), which is similar to bulk Cu_2O. Band structure calculations show a 2.95 eV direct band gap in Cu_2O monolayer (figure 3(i)), which is also larger than the 2.17 eV band gap in its parent bulk material. In contrast to the indirect bandgap in D-type CuO monolayer, the 2.95 eV direct bandgap makes the Cu_2O monolayer a possible material for sunlight harvesting applications. The indirect-to-direct bandgap transition between the D-type CuO monolayer and Cu_2O monolayer also suggests that the optical properties of a copper oxide thin film can be tuned by controlling the copper/

oxygen ratio, which can be implemented by various techniques such as controlling the oxygen pressure during the growth process.

As shown in supplementary figure S8, with all the three functionals we used (LDA+U, PBE+U, and HSE06), difference between measured d_{Cu-Cu} and calculated d_{Cu-Cu} in CuO is ~1%, while the difference between experimental d_{Cu-Cu} and calculated d_{Cu-Cu} in Cu_2O is larger than 5%. Considering the good agreement between the calculated Cu–O bond length and the experimental value (less than 0.2% discrepancy in HSE06 calculations), we can conclude that the as-fabricated copper oxide patch is CuO rather than Cu_2O.

Conclusion

In summary, a new monolayer oxide material, a single-atom-thick copper oxide nanosheet, has been fabricated. As new wide-bandgap semiconductors with a band gap of ~3 eV, single-atom-thick monolayer CuO and Cu_2O may also be candidates for high-power and high-temperature devices. In addition, the indirect-to-direct bandgap transition going from D-type CuO to Cu_2O monolayer holds promise in applications in optoelectronics where the optical properties of copper oxide monolayer can be tuned by modulating the oxygen content. This new material also provides an opportunity to understand the superconductivity mechanism in Cu-based oxides in which a planar copper oxide layer is believed to play the key role.

Methods

Graphene TEM sample preparation and process

Graphene was grown on copper foil using a standard chemical vapor deposition (CVD) method [27, 28]. The growth was carried out at low pressure with methane: hydrogen = 50 sccm: 50 sccm, at 1000 °C. The growth time was 20 min, which led to continuous few-layer graphene. After CVD growth, PMMA was spin-coated onto the graphene film, and the copper substrate was etched using a 10% ammonium persulfate ($(NH_4)_2S_2O_8$) with HCl solution instead of $FeCl_3$. After etching, the sample was washed with de-ionized water several times. The graphene film with PMMA was then scooped using a holey carbon TEM grid and was baked at 80 °C for better adhesion. The PMMA layer was then dissolved in acetone, and the TEM sample was further annealed at 300 °C under hydrogen flow to remove PMMA residuals. The graphene TEM sample was stored in air for a few months, and was baked under vacuum at 160 °C for 8 h before the STEM experiments. The sample further underwent a beam-shower process (i.e. high dose electron beam irradiation) before the *in situ* fabrication of the copper oxide monolayers. This preparation and process method produced a large amount of oxidized Cu nanoparticles (supplementary figure S1) and smaller Cu_xO clusters (supplementary figure S2) on graphene surface. Thus, graphene can be seen as a sample holder [29].

Aberration corrected STEM experiment

The *in situ* fabrication and characterization of monolayer copper oxide was carried out using a Nion UltraSTEM 100 operated at 60 kV. The microscope is fitted with an ultrahigh vacuum system, a cold field emission electron source, a corrector of third and fifth order aberrations, and equipped with an Enfina EEL spectrometer. The probe current was around 20 pA with a probe size about 1.3 Å in full-width-at-half-maximum (FWHM). The probe convergence half-angle was set to about 30 mrad, and the EELS collection angle was about 48 mrad. The ADF images were collected from 56–200 mrad or 80–200 mrad (when collected simultaneously with EELS). All the STEM-ADF images were low-pass filtered to improve the signal to noise ratio. Figure 2(b) is summed from 38 time-series images after correcting for sample drifting to clearly show the atomic structure of monolayer graphene.

Theoretical calculations

Quantum mechanical calculations were carried out based on DFT, projector augmented waves [30], and a plane wave basis set as implemented in the Vienna *Ab initio* Simulation Package [31]. For free-standing monolayer calculations, we employed the latest hybrid functional, HSE06, in which a portion $\alpha = 25\%$ of exact nonlocal Hartree–Fock exchange is mixed [32]. The energy cutoff of the plane-wave basis sets was 520 eV. k-point samplings in the Brillouin zone were fully tested to converge the energy to 1 meV/atom. Atoms were relaxed until the net force was less than 0.01 eV $Å^{-1}$. With these set of parameters, the calculated Cu–O bond length is 1.95 and 1.85 Å in CuO and Cu_2O bulk (experimental values are 1.96 and 1.85 Å). The excellent agreement between the calculations and experiments allows us to use the calculated Cu–Cu distance for monolayer CuO and Cu_2O to identify the observed copper-oxides structures as CuO. For the calculations which are too big to use hybrid functional, such as phonon dispersion and copper oxide patch on a graphene substrate, we use the local density approximation (LDA) [33]. An effective $U = 6.52$ eV on-site Coulomb interaction was applied to Cu in the Dudarev form [34], which is widely used for copper oxide systems [13]. The phonon properties were obtained by calculating the dynamical matrix with the finite-displacement method, with each displacement at 0.015 Å. The total energy is converged to 10^{-8} eV for the phonon calculations. Other functionals were also tested to make further assessment. Details of comparison are listed in supplementary figure S8.

Acknowledgments

Electron microscopy experiments and data analysis were performed at Oak Ridge National Laboratory under support from the US Department of Energy, Office of Science, Basic Energy Sciences, Materials Sciences and Engineering Division (KY, WZ, and MFC), and through a user project at ORNL's Center for Nanophase Materials Sciences (CNMS), which is a DOE Office of Science User Facility. Theoretical calculations were supported by US DOE Office of Basic Energy Sciences, Grant No. DE-FG02-09ER46554 (YYZ and STP). Supercomputer time was provided by the National Center for Supercomputing Applications and Extreme Science and Engineering Discovery Environment (XSEDE) and by the National Energy Research Scientific Computing Center, which is funded by the Department of Energy. Sample preparation and preliminary characterization were performed at Southeast University (YZ, KY and LS) under support from the National Natural Science Foundation of China (Nos. 11674052, 51420105003, 61274114, and 11327901), the national science fund for distinguished young scholars (No. 11525415), the Fundamental Research Funds for the Central Universities (Nos. 2242016K41039, MTEC-2015M03 and NJ20150026), and the Natural Science Foundation of Jiangsu Province (No. BK2012123). We thank Junhao Lin, Xiaohui Hu, Qian He, Miaofang Chi, Juan-Carlos Idrobo, and Andrew Lupini for useful discussions.

Competing financial interests

The authors declare no competing financial interests.

Author contributions

KY and WZ performed the electron microscopy experiments. WZ, KY and MFC analyzed the microscopy data. YYZ and STP carried out the theoretical calculations. YZ, KY and LS prepare the TEM sample and carried out preliminary characterization. YYZ, WZ and KY wrote the paper with help from MFC and STP.

References

[1] Ma R and Sasaki T 2010 Nanosheets of oxides and hydroxides: ultimate 2D charge-bearing functional crystallites *Adv. Mater.* **22** 5082

[2] Osada M and Sasaki T 2012 Two-dimensional dielectric nanosheets: novel nanoelectronics from nanocrystal building blocks *Adv. Mater.* **24** 210

[3] Sasaki T, Watanabe M, Hashizume H, Yamada H and Nakazawa H 1996 Macromolecule-like aspects for a colloidal suspension of an exfoliated titanate pairwise association of nanosheets and dynamic reassembling process initiated from it *J. Am. Chem. Soc.* **118** 8329

[4] Kim D S, Ozawa T C, Fukuda K, Ohshima S, Nakai I and Sasaki T 2011 Soft-chemical exfoliation of $Na_{0.9}Mo_2O_4$: preparation and electrical conductivity characterization of a molybdenum oxide nanosheet *Chem. Mater.* **23** 2700

[5] Surnev S, Vitali L, Ramsey M G, Netzer F P, Kresse G and Hafner J 2000 Growth and structure of ultrathin vanadium oxide layers on Pd(111) *Phys. Rev.* B **61** 13945

[6] Orzali T, Casarin M, Granozzi G, Sambi M and Vittadini A 2006 Bottom-up assembly of single-domain titania nanosheets on (1x2)-Pt(110) *Phys. Rev. Lett.* **97** 156101

[7] Tusche C, Meyerheim H L and Kirschner J 2007 Observation of depolarized ZnO(0001) monolayers: formation of unreconstructed planar sheets *Phys. Rev. Lett.* **99** 026102

[8] Addou R, Dahal A and Batzill M 2013 Growth of a two-dimensional dielectric monolayer on quasi-freestanding graphene *Nat. Nanotechnol.* **8** 41

[9] Quang H T, Bachmatiuk A, Dianat A, Ortmann F, Zhao J, Warner J H, Eckert J, Cunniberti G and Rümmeli M H 2015 *In situ* observations of free-standing graphene-like mono- and bilayer ZnO membranes *ACS Nano* **9** 11408

[10] Ruiz E, Alvarez S, Alemany P and Evarestov R A 1997 Electronic structure and properties of Cu_2O *Phys. Rev.* B **56** 7189–96

[11] Kastner M A, Birgeneau R J, Shirane G and Endoh Y 1998 Magnetic, transport, and optical properties of monolayer copper oxides *Rev. Mod. Phys.* **70** 897–928

[12] Ghijsen J, Tjeng L H, van Elp J, Eskes H, Westerink J, Sawatzky G A and Czyzyk M T 1988 Electronic structure of Cu_2O and CuO *Phys. Rev.* B **38** 11322–30

[13] Heinemann M, Eifert B and Heiliger C 2013 Band structure and phase stability of the copper oxides Cu_2O, CuO, and Cu_4O_3 *Phys. Rev.* B **87** 115111

[14] Reitz J B and Solomon E I 1998 Propylene oxidation on copper oxide surfaces: electronic and geometric contributions to reactivity and selectivity *J. Am. Chem. Soc.* **120** 11467–78

[15] Nakaoka K, Ueyama J and Ogura K 2004 Photoelectrochemical behavior of electrodeposited CuO and Cu_2O thin films on conducting substrates *J. Electrochem. Soc.* **151** C661–5

[16] Kim S Y, Ahn C H, Lee J H, Kwon Y H, Hwang S, Lee J Y and Cho H K 2013 p-channel oxide thin film transistors using solution-processed copper oxide *ACS Appl. Mater. Interfaces* **5** 2417–21

[17] Wöll C, Wilson R J, Chiang S, Zeng H C and Mitchell K A R 1990 Oxygen on cu(100) surface structure studied by scanning tunneling microscopy and by low-energy-electron-diffraction multiple-scattering calculations *Phys. Rev.* B **42** 11926–9

[18] Gong Y S, Lee C and Yang C K 1995 Atomic force microscopy and Raman spectroscopy studies on the oxidation of Cu thin films *J. Appl. Phys.* **77** 5422–5

[19] Samarasekara P, Kumara N T R N and Yapa N U S 2006 Sputtered copper oxide (CuO) thin films for gas sensor devices *J. Phys. Condens. Matter* **18** 2417

[20] Gattinoni C and Michaelides A 2015 Atomistic details of oxide surfaces and surface oxidation: the example of copper and its oxides *Surf. Sci. Rep.* **70** 424–47

[21] Gao S, Sun Y, Lei F, Liu J, Liang L, Li T, Pan B, Zhou J and Xie Y 2014 Freestanding atomically-thin cuprous oxide sheets for improved visible-light photoelectrochemical water splitting *Nano Energy* **8** 205

[22] Krivanek O L *et al* 2010 Atom-by-atom structural and chemical analysis by annular dark-field electron microscopy *Nature* **464** 571

[23] Zhou W, Oxley M P, Lupini A R, Krivanek O L, Pennycook S J and Idrobo J-C 2012 Single atom microscopy *Microsc. Microanal.* **18** 1342

[24] Egerton R F, Li P and Malac M 2004 Radiation damage in the TEM and SEM *Micron* **35** 399

[25] Zhao J, Deng Q, Bachmatiuk A, Sandeep G, Popov A, Eckert J and Rümmeli M H 2014 Free-standing single-atom-thick iron membranes suspended in graphene pores *Science* **343** 1228

[26] Zhang Y Y, Mishra R, Pennycook T J, Borisevich A Y, Pennycook S J and Pantelides S T 2015 Oxygen disorder, a way to accommodate large epitaxial strains in oxides *Adv. Mater. Interfaces* **2** 1500344

[27] Suk J W, Kitt A, Magnuson C W, Hao Y, Ahmed S, An J, Swan A K, Goldberg B B and Ruoff R S 2011 Transfer of CVD-Grown monolayer graphene onto arbitrary substrates *ACS Nano* **5** 6916
[28] Lee W H *et al* 2012 Simultaneous transfer and doping of CVD-grown graphene by fluoropolymer for transparent conductive films on plastic *ACS Nano* **6** 1284
[29] Pantelic R S, Suk J W, Hao Y, Ruoff R S and Stahlberg H 2011 Oxidative doping renders graphene hydrophilic, facilitaing its use as a support in biological TEM *Nano Lett.* **11** 4319
[30] Blochl P E 1994 Projector augmented-wave method *Phys. Rev.* B **50** 17953–79
[31] Kresse G and Furthmüller J 1996 Efficiency of ab-initio total energy calculations for metals and semiconductors using a plane-wave basis set *Comput. Mater. Sci.* **6** 15–50
[32] Heyd J, Scuseria G E and Ernzerhof M 2003 Hybrid functionals based on a screened coulomb potential *J. Chem. Phys.* **118** 8207–15
[33] Ceperley D M and Alder B J 1980 Ground state of the electron gas by a stochastic method *Phys. Rev. Lett.* **45** 566–9
[34] Dudarev S L, Botton G A, Savrasov S Y, Humphreys C J and Sutton A P 1998 Electron-energy-loss spectra and the structural stability of nickel oxide: an LSDA+U study *Phys. Rev.* B **57** 1505–9